Transient Detection of Spin-Labeled Myosin Subfragment 1 Conformational States during ATP Hydrolysis†

E. Michael Ostap,‡ Howard D. White,§ and David D. Thomas*,‡

Department of Biochemistry, University of Minnesota Medical School, Minneapolis, Minnesota 55455, and Department of Biochemistry, Eastern Virginia Medical School, Norfolk, Virginia 23501

Received February 1, 1993; Revised Manuscript Received April 15, 1993

ABSTRACT: We have used time-resolved electron paramagnetic resonance spectroscopy and caged ATP to detect nucleotide-induced changes in the conformational state of spin-labeled myosin heads (IASL-S1). Changes in the internal rotational dynamics of IASL-S1 were monitored with millisecond time resolution during the pre-steady-state phase of ATP hydrolysis. The changes in the internal protein dynamics were rigorously correlated with specific biochemical kinetic transitions, allowing us to observe directly the dynamic sequence of structural changes in IASL-S1 during the binding and hydrolysis of ATP. When caged ATP was photolyzed (producing 500 μM ATP) in the presence of 100 μM IASL-S1, the EPR signal intensity rose transiently to the steady-state ATPase level, indicating increased rotational motion about the SH_1 region of the myosin head. Kinetic and spectral analyses have resolved two phases of this transient, one representing the population of the M*·ATP state and the other representing the population of the M**·ADP·P_i state. We conclude that two motionally distinct states of the myosin head are present during ATP hydrolysis and that these states represent distinct conformational states that can be correlated with specific biochemical intermediates. Since specific labeling of myosin heads with IASL has been achieved in skinned muscle fibers, this study establishes the feasibility for the first direct detection and resolution of myosin's conformational transients during muscle contraction.

The molecular mechanism of muscle contraction involves the direct interaction of myosin and actin, coupled to the hydrolysis of adenosine 5′-triphosphate (ATP). According to the rotating cross-bridge model, the pivoting motion of the myosin head attached to actin produces strain, which is then relieved by the sliding motion of the myosin and actin filaments (Reedy et al., 1965; Huxley, 1969; Huxley & Simmons, 1971). The general hypothesis is that changes in the nucleotide at the myosin active site induce changes in the conformation of the myosin head, which change the interaction between myosin and actin in a way that results in directional sliding of the filaments (Taylor, 1979; Eisenberg & Hill, 1985; Hibberd & Trentham, 1986).

Conformational changes within the myosin head during steady-state ATP hydrolysis have been detected by observing changes in the UV absorbance (Morita, 1967), intrinsic fluorescence (Werber et al., 1972; Bagshaw & Trentham, 1974; Trentham et al., 1976), biochemical cross-linking (Sutoh & Lu, 1987; Huston et al., 1988), electron paramagnetic resonance (EPR)[1] spectroscopy (Seidel et al., 1970; Wells & Bagshaw, 1984; Barnett & Thomas, 1987), electron microscopy (Walker & Trinick, 1988; Katayama, 1989; Tokunaga et al., 1991), NMR spectroscopy (Shriver & Sykes, 1982), fluorescently labeled SH_2 (Hiratsuka, 1992), fluorescence energy transfer (Dalbey et al., 1983), and small-angle X-ray scattering (Wakabayashi et al., 1992). The goal of these studies has been to correlate structural changes with specific kinetic intermediates and the force-generating step. To achieve this goal, distinct conformational states of the myosin head must be resolvable, and it must be possible to quantitate the mole fractions of these states during the ATP hydrolysis cycle. The technique should also site-specifically detect changes only in the myosin head, so the study can be extended to muscle fibers.

Because EPR spectroscopy can be used to (a) resolve more than one motionally distinct class of spin-labels, (b) quantitate precisely the relative concentrations of the motional classes, and (c) study myosin heads specifically in skinned fibers as well as in isolated myosin (Thomas & Cooke, 1980; Matta & Thomas, 1992), it is ideally suited to the study of the conformational states of the myosin head during ATP hydrolysis and muscle contraction.

EPR spectroscopy of myosin heads labeled at Cys-707 (SH_1) with IASL (IASL-myosin) has demonstrated the presence of motionally distinct states that are dependent on the nucleotide at the myosin active site (Seidel & Gergely, 1971; Barnett & Thomas, 1987). In the absence of nucleotides, the EPR spectrum reports the rigid, stereospecific attachment of spin-labels to the myosin heads (Thomas & Cooke, 1980; Barnett & Thomas, 1987). The addition of ADP to myosin slightly mobilizes the spin-label relative to the myosin head, and ATP mobilizes the probe much more (Seidel & Gergely, 1973; Barnett & Thomas, 1987). Barnett and Thomas (1987) investigated the nucleotide-dependent changes in the conventional EPR spectrum during steady-state ATP hydrolysis, and assigned the two motional classes observed during steady-

† This work was supported by grants to D.D.T. from the National Institutes of Health (AR 39754) and the Minnesota Supercomputer Institute. E.M.O. was supported by a predoctoral training grant from the NIH (GM 08277-03). H.D.W. was supported by a grant from the NIH (HL-41776).

* To whom correspondence should be addressed.
‡ University of Minnesota Medical School.
§ Eastern Virginia Medical School.

[1] Abbreviations: caged ATP, P^3-[1-(2-nitrophenyl)ethyl]adenosine 5′-triphosphate; CP, creatine phosphate; CPK, creatine kinase; TPX, tetramethylene polymer plastic; EDTA, ethylenediaminetetraacetic acid; EGTA, ethylene glycol bis(β-aminoethyl ether)-*N*,*N*,*N*′,*N*′-tetraacetic acid; EPPS, *N*-(2-hydroxyethyl)piperazine-*N*′-3-propanesulfonic acid; EPR, electron paramagnetic resonance; KPr, potassium propionate; IASL, 4-(2-iodoacetamido)-2,2,6,6-tetramethyl-1-piperidinyloxy; MOPS, 3-(*N*-morpholino)propanesulfonic acid; P_i, inorganic phosphate; S1, chymotryptic myosin subfragment 1; SH_1, myosin Cys-707; SH_2, myosin Cys-697; V_i, Na_3VO_4; τ_r, rotational correlation time; τ_r^{eff}, effective rotational correlation time; $2T_{\parallel}'$, spectral splitting.

0006-2960/93/0432-6712$04.00/0

Table I: Buffers for Steady-State and Transient EPR Experiments[a]

	[nucleotide]	[V_i]	[CP]	[CPK]	[$MgCl_2$]	[KPr]	[EGTA]	[buffer][b]
no nucleotide					6.0	135	1.0	20.0
ATP + backup	5.0		20.0	233	6.0	60	1.0	20.0
ADP	5.0				6.0	124	1.0	20.0
ADP + V_i[c]	5.0	5.0			6.0	64	1.0	20.0
5 mM caged ATP	5.0				6.0	124	1.0	20.0

[a] Concentrations are in millimolar. The CPK concentration is in international units per milliliter. The pHs of the buffers were adjusted at 22 °C. [b] MOPS was used for pH 7.0, and EPPS was used for pH 8.0. [c] ADP + V_i experiments were performed at pH 8.0.

state ATP hydrolysis to the M* and M** states of the myosin head. However, to correlate rigorously the motionally distinct states with kinetic states in the myosin ATPase cycle, the motionally distinct states must be studied during the pre-steady-state phase of ATP hydrolysis and compared directly with transient biochemical kinetics.

We have developed a technique to study EPR signals during the pre-steady-state phase of ATP hydrolysis. EPR signals are monitored transiently on the millisecond time scale as ATP is rapidly introduced into the sample by the photolysis of caged ATP (Berger et al., 1989; Fajer et al., 1990; Ostap & Thomas, 1991). In the present study, we have used steady-state and transient EPR to detect specific conformational states in the myosin head and have directly correlated these states with specific kinetic intermediates in the myosin ATPase cycle.

MATERIALS AND METHODS

Preparations and Solutions. Chymotryptic myosin subfragment 1 (S1) was prepared as described by Eads et al. (1984), except that the chymotryptic digestion time was 10 min. S1 was spin-labeled with 4-(2-iodoacetamido)-2,2,6,6-tetramethyl-1-piperidinyloxy (IASL) as described for myosin by Barnett and Thomas (1987), except that unreacted spin-label was removed by dialysis. After spin-labeling, IASL-S1 was stored in liquid nitrogen. The concentration of IASL-S1 was determined spectrophotometrically at 280 nm, using an extinction coefficient of 0.74 $(mg/mL)^{-1}$ cm^{-1} (Margossian & Lowey, 1982). IASL-S1 was purified before spectroscopy by HPLC on a preparative Bio-Rad (Richmond, CA) MA7Q anion-exchange column (2 cm × 10 cm) and eluted in 20 mM imidazole, pH 7.0, with a linear gradient of 0–0.5 M NaCl. The major protein peak was saved. The other fractions did not have significant ATPase activity. This purification removed nucleotide-insensitive S1, as determined by EPR, from the preparation. The S1 was concentrated using Centricon-30 concentrators (Amicon, Beverly, CA) and then diluted into the appropriate buffer.

All buffers were prepared as described in Table I. Potassium propionate (KPr) was added to achieve the desired ionic strength. A stock solution of 200 mM Na_3VO_4 (V_i) was prepared as described by Barnett and Thomas (1987). Caged ATP (CalBiochem, San Diego, Ca) was purified by HPLC on a preparative Bio-Rad MA7Q anion-exchange column (2 cm × 10 cm) and eluted with a linear gradient of 0–2.0 M triethylamine bicarbonate, pH 7.8 (Berger & Thomas, 1991). The eluted caged ATP was then lyophilized, resuspended in distilled water, lyophilized again, and diluted to a final concentration of 50–100 mM. The caged ATP concentration was determined spectrophotometrically at 260 nm, using an extinction coefficient at 18 900 M^{-1} cm^{-1}.

Characterization of Spin-Labeled S1. The extent and specificity of SH_1 (Cys-707) labeling were determined by measuring high-salt ATPase activities and double integration of EPR spectra. ATPase activities were determined by measuring the production of inorganic phosphate (Lanzetta, 1979). The K/EDTA-ATPase activity was assayed at 25 °C in a solution containing 5 mM EDTA, 0.60 M KCl, and 50 mM MOPS, pH 7.5. The Ca/K-ATPase activity was assayed at 25 °C in a solution containing 10 mM $CaCl_2$, 0.60 M KCl, and 50 mM MOPS, pH 7.5. The molar concentration of spins was determined by the double integration of digitized EPR spectra, calibrated with a standard spin-label solution prepared from the same stock solution used for labeling.

Transient Kinetics and Simulations. The rates of ATP binding and ATP hydrolysis were determined by stopped-flow fluorescence measurements as described previously (Johnson & Taylor, 1978; Sleep et al., 1981). The equilibrium constants for the ATP hydrolysis reaction at pH 7.0 and 8.0 were determined by quench flow experiments as described previously (Johnson & Taylor, 1978; White, 1982). The rate of phosphate release was determined and calculated by single-turnover and steady-state experiments as described previously (Lanzetta et al., 1979; Johnson & Taylor, 1978; Sleep et al., 1981; White, 1982). The rate of ADP dissociation was determined by measuring the rate of increase of the fluorescence signal due to the reaction of the IASL-S1–ADP complex with excess ATP as described previously (Sleep et al., 1981).

Kinetic simulations were performed on an IBM-compatible computer using a program (KSIM) written by N. C. Millar. This program solves differential rate equations by numerical integration using the Runge–Kutta algorithm (Press et al., 1987). Because experimental EPR transients were acquired with a time constant of 5.12 ms, the fastest EPR transient that could be detected is 195 s^{-1}. The kinetic simulations were compared directly to experimental EPR transients (see Results), so the kinetic simulations must be filtered at the same time constant as the EPR experiments. This was accomplished by filtering the kinetic simulations at pH 7.0 and 8.0 with a time constant of 5.12 ms.

Steady-State and Transient EPR Spectroscopy. EPR experiments were performed on a Bruker ESP 300 spectrometer (Bruker Instruments, Billerica, MA) using a TE_{102} EPR cavity (ER4102 ST; Bruker Instruments), with samples contained in a 20-μL well on a TPX cover plate that was attached to a quartz–Suprasil flat cell (WG-807; Wilmad, Buena, NJ). The peak-to-peak modulation amplitude was 5 G, and the microwave field intensity was 0.144 G, as calculated from cavity Q and peroxylamine disulfonate (PADS) calibrations (Squier & Thomas, 1986). The temperature of the samples was maintained by using a variable-temperature controller (ER4111; Bruker Instruments). All spectra were acquired at 22 ± 1.0 °C, unless stated otherwise. Transient EPR spectra were obtained at a single field position defined by the low-field peak of the mobile component (see Results). Transient EPR spectra were acquired with a 2.56-ms dwell time and a 5.12-ms filter time constant. Caged ATP was photolyzed during EPR experiments by a single 10-ns burst of 351-nm light from a XeF excimer laser (LPX200i, Lambda Physik, Acton, MA). The light was introduced directly into the optical port of the EPR cavity. A small spike (<10% of

Scheme I

$$\text{CATP} \xrightarrow{k_{caged}} \text{ATP} + \text{M} \underset{}{\overset{K_1}{\rightleftharpoons}} \text{M}\cdot\text{ATP} \overset{k_2}{\rightleftharpoons} \text{M}^*\cdot\text{ATP} \overset{k_3}{\rightleftharpoons}$$

$$\text{M}^{**}\cdot\text{ADP}\cdot\text{P}_i \overset{k_4}{\rightleftharpoons} \text{M}^*\cdot\text{ADP} \overset{k_5}{\rightleftharpoons} \text{M}$$

$$\text{P}_i \qquad\qquad \text{ADP}$$

the total signal change) sometimes occurred in the data upon the laser flash. This spike always decayed with the instrument filter time constant, and it does not affect the analysis of the data in this study. The TPX sample well was the same size as the optical port on the EPR cavity, so the entire sample was uniformly exposed. The light energy incident on the sample was measured with a thermal joule meter (Model 25A; Optical Engineering, Santa Rosa, CA) and was ~150 mJ/cm^2 for a single pulse.

EPR Data Analysis. EPR spectra were acquired and digitized with the spectrometer's built-in microcomputer using ESP 1620 spectral acquisition software (Bruker Instruments). Digitized EPR spectra were analyzed on IBM-compatible computers using a program developed by Robert L. H. Bennett. Transient EPR spectra were fitted to one or two exponentials by a nonlinear least-squares curve fit using the Marquardt method (Press et al., 1986). All spectra were normalized to correspond to the same number of spins by dividing by the double integral of the EPR spectrum. Each EPR transient was divided by the double integral of the conventional EPR spectrum acquired before caged ATP photolysis. Spectral subtractions were performed as described by Barnett and Thomas (1987). Effective rotational correlation times (τ_r) that assume isotropic rotational motion were determined by comparison of spectral splittings, $2T_\parallel'$ (Figure 2), with calibration curves (McCalley et al., 1972; Thomas et al., 1975). Apparent order parameters (S) were calculated to describe rapid restricted motion by $S = (T_\parallel' - T_0)/(T_\parallel - T_0)$, where T_0 is the isotropic hyperfine splitting constant (Squire et al., 1989). When rapid restricted motion was assumed, the half-cone angle (θ_c) that describes the amplitude of the motion was calculated from the order parameter by $S = {}^1/_2(\cos\theta_c + \cos^2\theta_c)$.

RESULTS

Labeling Specificity. The reaction of IASL with myosin has been shown to be very specific for Cys-707 (SH_1) under the described labeling conditions (Barnett & Thomas, 1987). The modification of SH_1 is known to cause changes in the S1 high-salt ATPase activity (Sekine & Kielly, 1964; Crowder & Cooke, 1984). The inhibiton of the K/EDTA-ATPase activity has been demonstrated to be a sensitive indicator of the fraction of SH_1 and/or SH_2 (Cys-697) groups modified, declining linearly with the increase in the percentage of heads with either or both of these SH groups modified. Also, specific modification of SH_1, and not SH_2, greatly increases the Ca/K-ATPase activity. In the IASL-S1 preparations used in this study, the K/EDTA-ATPase activity was inhibited by 0.97 ± 0.01 (f_{SH}), and Ca/K-ATPase activity was increased 11 ± 1.0 times. Double integration of the EPR spectra showed that IASL-S1 contained 0.95 ± 0.08 spin-label per S1 (f_{SL}), so the calculated specificity (f_{SH}/F_{SL}) is 1.0 ± 0.09. Therefore, virtually every S1 in the preparations used in this study was specifically labeled at SH_1 (not SH_2).

Transient ATPase Kinetics. There are three major perturbations of the myosin ATPase cycle (Scheme I) caused by the covalent modification of SH_1 with iodoacetamide: (a) a decrease in the rate ($k_{+3} + k_{-3}$) of ATP hydrolysis; (b) a decrease in the equilibrium constant (K_3) of the ATP hydrolysis step; and (c) an increase in the rate of the product release step (k_4) (Sleep et al., 1981). To determine whether the IASL-labeled S1 preparation used in this study was kinetically equivalent to the iodoacetamide-labeled S1 preparation used by Sleep et al. (1981), transient kinetic experiments were performed on IASL-S1 as described previously (Johnson & Taylor, 1978; Sleep et al., 1981; White, 1982).

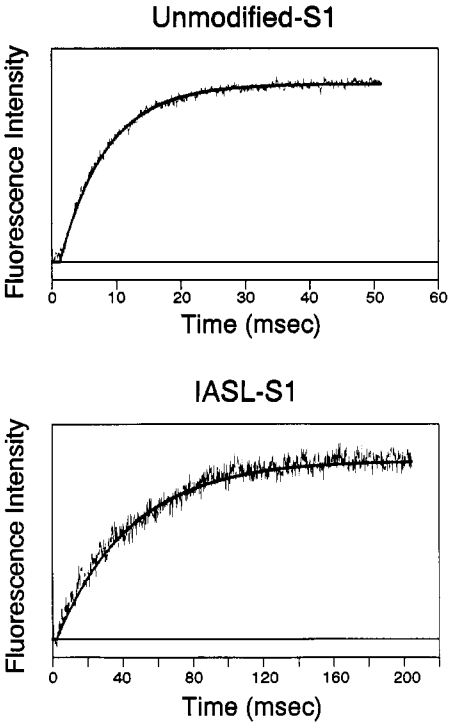

FIGURE 1: Stopped-flow records of S1 fluorescence during the reaction of 2.5 μM unmodified S1 (top) and 2.5 μM IASL-S1 (bottom) with 250 μM ATP at pH 7.0. The solid lines are single-exponential fits to the fluorescence data with rates of 150 s^{-1} (top) and 25 s^{-1} (bottom).

Figure 1 shows typical stopped-flow S1 fluorescence data used for determination of the rate of ATP hydrolysis at pH 7.0. The rate of ATP hydrolysis ($k_3 + k_{-3}$) for the unmodified S1 (150 s^{-1}) was much greater than that for IASL-S1 (25 s^{-1}). This is also true at pH 8.0 (data not shown, see rate constants below). The equilibrium constants for the ATP hydrolysis reaction (K_3) were determined at pH 7.0 and 8.0 by quench flow experiments. The phosphate burst at pH 7.0 was 0.35 ± 0.04, and 0.45 ± 0.06 at pH 8.0 (data not shown).

The simplified ATPase reaction is shown in Scheme I, and the steps are numbered as in Sleep et al. (1981). The rate constants determined from the transient kinetic experiments for IASL-S1 are as follows at pH 7.0: $K_1k_2 = 3 \times 10^6$ s^{-1} M^{-1}, $k_{+3} = 9$ s^{-1}, $k_{-3} = 16$ s^{-1}, $k_4 = 1.7$ s^{-1}, and $k_5 = 10$ s^{-1}. The rate constants are as follows at pH 8.0: $K_1k_2 = 3 \times 10^6$ s^{-1} M^{-1}, $k_{+3} = 12$ s^{-1}, $k_{-3} = 14$ s^{-1}, $k_4 = 1.7$ s^{-1}, and $k_5 = 10$ s^{-1}. The photolysis rate of caged ATP at pH 7.0 is $k_{caged} = 100$ s^{-1}, and at pH 8.0 is $k_{caged} = 10$ s^{-1} (McCray et al., 1980; Goldman et al., 1984; Walker et al., 1988). Therefore, after the photolysis of 500 μM caged ATP, 100 μM IASL-S1 is saturated with ATP within 10 ms at pH 7.0 and within 35 ms at pH 8.0.

Steady-State EPR Spectra. Figure 2 shows the conventional EPR spectra of 100 μM IASL-S1 in the absence and the presence of nucleotides, and Table II shows the parameters derived from these spectra. In the absence of nucleotides, IASL is rigidly immobilized on the myosin head (Thomas et al., 1975; Barnett & Thomas, 1987). Therefore, the EPR

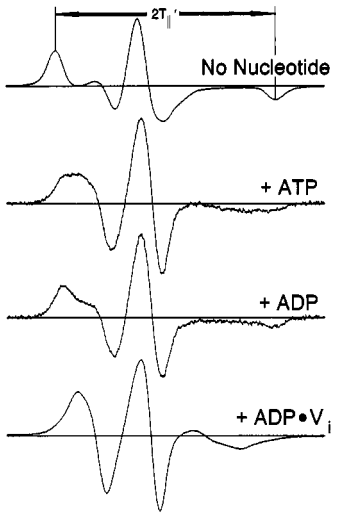

FIGURE 2: Steady-state EPR spectra of 100 μM IASL-S1 (first) in the absence of nucleotide, (second) in the presence of 5 mM ATP + 20 mM CP, (third) in the presence of 5 mM ADP, and (fourth) in the presence of 5 mM ADP and 5 mM V_i. The spectral splitting ($2T_{\parallel}'$) is defined in the top spectrum. All spectra are normalized to correspond to the same number of spins.

Table II: Spectral Splittings and Order Parameters[a]

sample[b]	$2T_{\parallel}'$	τ_r^{eff} [d]	S^{eff} [e]	θ_c^{eff} [f] (deg)
no nucleotide	69.75 ± 0.22 (11)	0.2 μs	1.0	0
caged ATP[c]	69.67 ± 0.07 (15)	0.2 μs	1.0	0
ADP	66.90 ■ 0.42 (26)	50 ns	0.92	20
ATP	NA	NA	NA	NA
ADP + V_i	51.46 ■ 0.48 (4)	9 ns	0.49	52

[a] $2T_{\parallel}'$ is defined in Figure 1. The number in parentheses is the number of combined experiments for determination of the mean and the standard deviation. NA indicates not applicable for those samples where more than one population of spins distorts the measurement of $2T_{\parallel}'$. [b] Splittings are independent of pH. [c] Spectral splitting of IASL-S1 prior to caged ATP photolysis. [d] Effective rotational correlation time, assuming isotropic ($S = 0$) rotational motion. [e] Effective order parameter assuming rapid ($\tau_r \leq 0.1$ ns) restricted rotational motion. [f] Half-cone angle for spin-label wobble, calculated from S^{eff}.

spectrum of IASL-S1 (Figure 2, top; Table II) reports the overall rotation of IASL-S1 in solution ($\tau_r = 0.2$ μs at 20 °C; Thomas et al., 1975), and not the rotation of the spin-label relative to S1.

When 5 mM ADP is added to 100 μM IASL-S1 (Figure 2, third spectrum), the splitting ($2T_{\parallel}'$) of the single-component EPR spectrum decreases (Table II), indicating an increase in the spin-label's submicrosecond rotational mobility (Seidel et al., 1970; Seidel & Gergely, 1971; Barnett & Thomas 1987). ADP induces a 2.9-G decrease in $2T_{\parallel}'$, which corresponds to a decrease in the rotational correlation time from about $\tau_r = 0.2$ μs (Thomas et al., 1975) to $\tau_r^{eff} = 50$ ns, assuming isotropic rotational motion (McCalley et al., 1972). Alternatively, assuming rapid ($\tau_r \leq 0.1$ ns) restricted motion, the half-cone angle (θ_c) that describes the amplitude of the spin-label's rotational motion increases from 0 ° to $\theta_c^{eff} = 20°$ (Table II). Thus, the actual τ_r is ≤50 ns, and the actual θ_c is ≥20°. This increased rotational mobility is due to rotation of the spin-label relative to the myosin head, rather than to an overall increase in the rate of rotation of the myosin head (Barnett & Thomas, 1987).

When 5 mM ATP + 20 mM CP is added to 100 μM IASL-S1, the EPR spectrum (Figure 2, second spectrum) reports a linear combination of two populations of probes that are significantly more mobile than the probes in the absence of nucleotide (Seidel & Gergely, 1971; Seidel, 1975; Wells & Bagshaw, 1984; Barnett & Thomas, 1987). The component with the greater splitting (i.e., the more motionally restricted component) is identical to the single population of spin-labels observed when ADP is added to IASL-S1 (Barnett & Thomas, 1987). The second component is significantly more mobile, corresponding to $\tau_r \leq 9$ ns and $\theta_c \geq 52°$ (Table II). These two motional classes represent two distinct local conformations of the myosin head that are in slow exchange with one another during the ATP hydrolysis reaction cycle (Barnett & Thomas, 1987).

The addition of ATP and orthovanadate (V_i) to S1 traps the myosin head in a complex that has been proposed to be a conformational analog of the complex M·ADP·P_i, a key intermediate in the ATP hydrolysis reaction (Goodno, 1979; Dantzig & Goldman, 1985). It has been demonstrated previously that the addition of ADP + V_i or ATP + V_i to IASL-labeled myosin heads induces a mobilization of the spin-label that is even greater than that observed in the presence of ATP (Wells & Bagshaw, 1984; Barnett & Thomas, 1987). The spectrum of 100 μM IASL-S1 + 5 mM ADP + 5 mM V_i is shown (Figure 2, bottom spectrum). This spectrum is indistinguishable from the spectrum of 100 μM IASL-S1 + 5 mM ATP + 5 mM V_i (data not shown). Both the ADP-like component and the highly mobile component are present in the S1·ADP·V_i spectrum (Figure 2, bottom spectrum), but the highly mobile component is more highly populated than in the presence of ATP (Barnett & Thomas, 1987).

Resolution of Spectral Components. Conventional EPR has the sensitivity and resolution to (a) resolve motionally distinct classes of probes and (b) quantitate precisely the relative concentrations of the motional classes through spectral subtraction. In order to test rigorously whether all spectra of IASL-S1 do in fact correspond to a linear combination of two motionally distinct conformations, and in order to quantitate the mole fractions of these components under various conditions, we carried out digital spectral analysis to resolve and quantitate the spectral components. For the remainder of this paper, the ADP-like component will be referred to as the immobile component, and the other will be called the mobile component (Barnett & Thomas, 1987).

Using the spectrum of IASL-S1 + ADP (Figure 3, center spectrum) as a model for the immobile component, computer subtraction was used to quantitate the relative concentrations of the two components in the ADP + V_i spectrum (Figure 3, Table III). The immobile component (Figure 3, center) was subtracted from the ADP + V_i (Figure 3, top) spectrum until the intensity from the spectral wings was removed without distorting the central line. This procedure results in a well-defined, unambiguous end point (Figure 3, bottom), as shown previously for IASL-myosin (Barnett & Thomas, 1987), which is used as the mobile component in subsequent analyses. The results of this analysis (Table III) show that the spectrum is composed of 16 ± 2.2% of the immobile component and 84 ± 2.2% of the mobile component. As determined previously for IASL-myosin (Barnett & Thomas, 1987), the spectrum of the mobile component (Figure 3, bottom) implies rapid ($\tau_r \leq 9$ ns) and large-amplitude ($\theta_c \geq 52°$) rotational motion (Table II).

The spectrum of IASL-S1 + ATP has the same two motional components as the spectrum of IASL-S1 + V_i, but the fractions of the components are very different (Table III). At pH 7.0, subtraction of 69 ± 3.7% of the immobile component (Figure 4, center and left) from the ATP spectrum (Figure 4, top and left) results in a residual (Figure 4, bottom and left) that is indistinguishable from the mobile component derived from

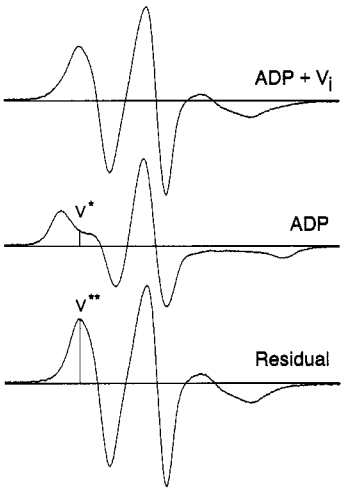

FIGURE 3: Spectral subtraction of 100 μM IASL-S1 + 5 mM ADP from 100 μM IASL-S1 + 5 mM ADP + 5 mM V_i. (Top) Steady-state EPR spectrum of 100 μM IASL-S1 + 5 mM ADP + 5 mM V_i. (Center) Steady-state EPR spectrum of 100 μM IASL-S1 + 5 mM ADP. (Bottom) Residual spectrum obtianed by the subtraction of 0.16 of the spectrum of IASL-S1 + ADP from that of IASL-S1 + ADP + V_i. All spectra are normalized to correspond to the same number of spins. The intensities, V^* and V^{**}, used in the simulation of EPR transient are defined.

Table III: Relative Populations of the Two Nucleotide-Induced Motional Components[a]

sample	% mobile	mobile/immobile
IASL-S1, pH 7.0		
ADP	0	0
ATP	31 ± 3.7 (5)	0.45 ± 0.06
IASL-S1, pH 8.0		
ADP	0	0
ATP	43 ± 1.4 (6)	0.75 ± 0.03
ADP + V_i	84 ± 2.2 (4)	5.3 ± 0.74

[a] The relative populations of the two components are determined by spectral subtractions. Mobile and immobile are defined in the text. The number in parentheses is the number of combined experiments, each from a different protein preparation, for the determination of the mean and the standard deviation.

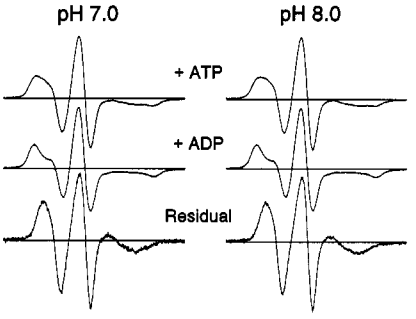

FIGURE 4: Spectral subtractions of 100 μM IASL-S1 + 5 mM ADP from 100 μM IASL-S1 + 5 mM ATP + 20 mM CP at pH 7.0 (left) and pH 8.0 (right). (Top) Steady-state EPR spectra of 100 μM IASL-S1 + 5 mM ATP + 20 mM CP. (Center) Steady-state EPR spectra of 100 μM IASL-S1 + 5 mM ADP. (Bottom) Residual spectra obtained by the subtraction of IASL-S1 + ADP from IASL-S1 + ATP (Table III). The residuals are identical to the corrected IASL-S1 + ADP + V_i spectrum (Figure 3, bottom). All spectra are normalized to correspond to the same number of spins.

the ADP + V_i spectrum (Figure 3, bottom). At pH 8.0, subtraction of 57 ± 1.4% of the immobile component (Figure 4, center and right) from the ATP spectrum (Figure 4, top and right) results in a residual (Figure 4, bottom and right) that is indistinguishable from the mobile component derived from the ADP + V_i spectrum (Figure 3, bottom). Because

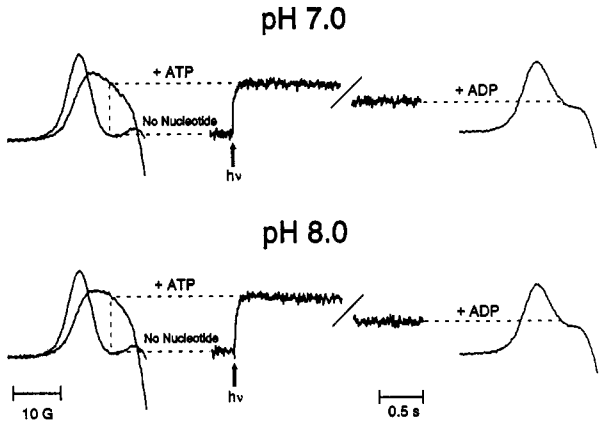

FIGURE 5: Steady-state and transient EPR spectra of 100 μM IASL-S1 at pH 7.0 (top) and pH 8.0 (bottom). (Left) Overlays of the low-field portion of steady-state EPR spectra of 100 μM IASL-S1 in the presence of 5 mM ATP + 20 mM CP or 5 mM caged ATP (no nucleotide). The dashed line identifies the field position monitored during transient EPR experiments. (Center) Transient EPR spectra of 100 μM IASL-S1 monitoring a single field position. 500 μM ATP was released in the sample at the laser pulse (arrow). (Right) The low-field portion of the steady-state EPR spectra after the depletion of ATP.

these spectra were acquired during steady-state ATP hydrolysis, the fractions of the two spectral components represent the relative concentrations of the two predominant biochemical intermediates present during steady-state ATP hydrolysis (Seidel & Gergely, 1973; Barnett & Thomas, 1987). Dividing the fraction of the mobile component by the fraction of the immobile component results in a ratio (pH 7.0, 0.45 ± 0.06; pH 8.0, 0.75 ± 0.03) that is essentially the same as the equilibrium constant (pH 7.0, $K_3 = 0.54$; pH 8.0, $K_3 = 0.82$) determined by quench flow experiments for the ATP hydrolysis step (Table III). This is expected, since the predominant intermediates during steady-state ATP hydrolysis are the M*·ATP and M**·ADP·P_i states (Scheme I). The immobile component has been assigned to a conformation of the myosin head that is in the M*·ATP state, and the mobile component has been assigned to a conformation of the myosin head that is in the M**·ADP·P_i state (Seidel & Gergely, 1973; Barnett & Thomas, 1987).

Transient EPR. Transient EPR studies allow us to correlate more rigorously the motionally distinct states with kinetic states in the S1 ATPase cycle. The populations of the two spectral components can be monitored during the pre-steady-state phase of ATP hydrolysis. The rate of appearance and the extent of population of the mobile component can be correlated with the rate and extent of population of a biochemical state obtained from kinetic simulations using known kinetic constants.

Figure 5 illustrates transient EPR experiments at pH 7.0 and pH 8.0. The low-field regions of the EPR spectra of IASL-S1 in the presence of 5 mM caged ATP (no nucleotide), and during steady-state ATP hydrolysis, are shown (Figure 5, left). The spectrum of IASL-S1 + caged ATP, before caged ATP photolysis, is not significantly different from the spectrum of IASL-S1 in the absence of nucleotides (Table II), indicating that the caged ATP preparation is free of contaminating ADP and ATP.

Because of the time resolution required for the study of the pre-steady-state phase of ATP hydrolysis, the entire EPR spectrum could not be acquired during the transient EPR experiment, so the intensity at a single field position in the spectrum was monitored transiently (Berger et al., 1989; Fajer et al., 1990; Ostap & Thomas, 1991). The field position

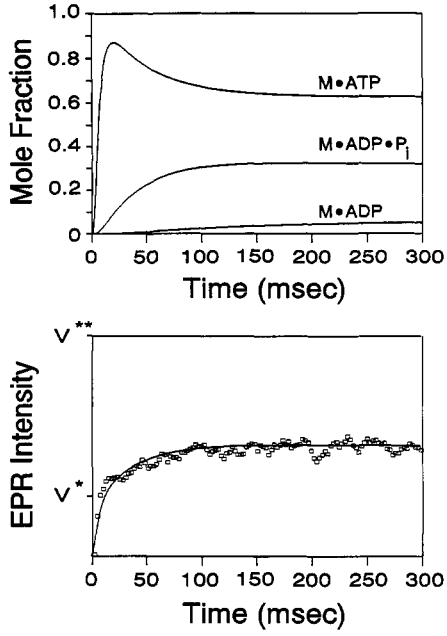

FIGURE 6: (Top) Transient kinetic simulations of the predominant intermediates of the IASL-S1 ATPase cycle at pH 7.0 assuming 100 μM IASL-S1 + 500 μM ATP. (Bottom, boxes) Expanded EPR transient (from Figure 4) showing individual data points (2.56 ms per point). (Bottom, line) Simulated EPR transient as defined in the text. The relative EPR intensities V^{**} and V^{*} are defined.

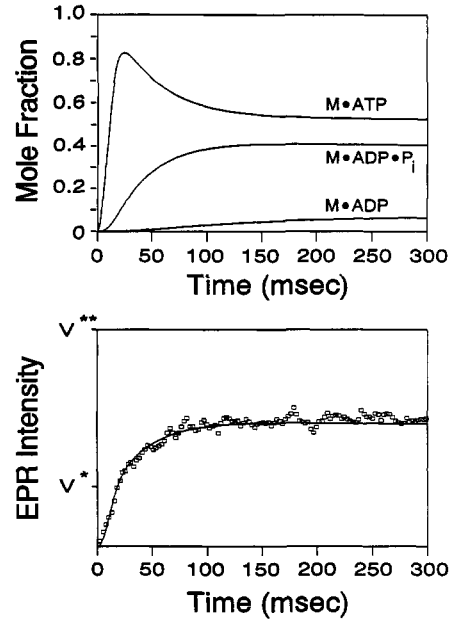

FIGURE 7: (Top) Transient kinetic simulations of the predominant intermediates of the IASL-S1 ATPase cycle at pH 8.0 assuming 100 μM IASL-S1 + 500 μM ATP. (Bottom, boxes) Expanded EPR transient (from Figure 4) showing individual data points (2.56 ms per point). (Bottom, line) Simulated EPR transient as defined in the text. The relative EPR intensities V^{**} and V^{*} are defined.

monitored was defined by the low-field peak of the mobile component (Figure 3). This position has no intensity in the absence of nucleotide, and is the most sensitive point in the spectrum to the population of the mobile component. However, the immobile component also contributes to the spectral intensity at this field position (Figure 3, center). Therefore, the total transient EPR signal at this field position (V^{tot}) is the sum of contributions from the immobile and mobile components. When the EPR spectrum reports that all of the IASL-S1 heads are populating the immobile component (e.g., the IASL-S1 + ADP spectrum), the intensity at this field position is defined as V^{*} (Figure 3, center). When the mobile component is completely populated (e.g., IASL-S1 + ADP·V_i minus the immobile component), the intensity at this field position is defined as V^{**} (Figure 3, bottom).

Before photolysis of the caged ATP, the intensity at this field position is identical to the intensity of the no-nucleotide sample ($V^{tot} = 0$). Immediately after photogeneration of 500 μM ATP, the EPR intensity rapidly increases to the level of the ATP spectrum (Figure 5, center), indicating the steady-state turnover of the ATP. After a brief steady-state (~5 s), the ATP is depleted, and the spectral intensity drops to the IASL-S1 + ADP level (Figure 5, right).

The time base of the EPR transients in Figure 5 has been expanded to show the changes in the EPR intensity during the pre-steady-state phases of ATP hydrolysis (Figures 6 and 7, bottom). Each point (open box) was acquired with a 2.56-ms dwell time and a 5.12-ms time constant. The 10-ns laser pulse of 351-nm light occurred at time zero. At pH 7.0 (Figure 6, bottom), two phases of the EPR transient are clearly resolved. The first phase of the EPR transient rises to the intensity of V^{*} within 10 ms, and the second, slower phase, reaches the steady-state level at a rate of 21 ± 2 s^{-1}. At pH 8.0 (Figure 7, bottom), the two phases are not as clearly resolved. The photolysis rate of caged ATP is 10× slower at pH 8.0 (McCray et al., 1980), limiting the rate of ATP binding to IASL-S1. This transient can be fit adequately to a single exponential with a rate of 31 ± 1 s^{-1}.

To determine whether the assignments of the mobile component to the M**·ADP·P_i state and the immobile component to the M*·ATP and M*·ADP states are correct, the experimental transients were compared to kinetic simulations. Simulations of the pre-steady-state phases of the predominant kinetic intermediates using rate constants defined previously are shown (Figures 6 and 7, top). As stated earlier, each EPR transient (V^{tot}) is assumed to be a linear combination of the mobile and immobile components. To make a direct comparison between the kinetic simulations with the EPR transients, normalized kinetic simulations, weighted by their respective contributions to the EPR transient (V^{*} and V^{**}), must be added, creating simulated EPR transients. Simulated EPR transients were constructed as follows:

$$V^{tot}(t) = V^{*}c^{*}(t) + V^{**}c^{**}(t)$$

where V^{tot}, V^{*}, and V^{**} are the previously defined EPR intensities, $c^{*}(t)$ is the mole fraction of S1 in the M*·ATP and M*·ADP states, and $c^{**}(t)$ is the mole fraction of S1 in the M**·ADP·P_i state at time t determined by the kinetic simulations.

When the mobile component is assigned to the M**·ADP·P_i state, and the immobile component is assigned to the M*·ATP and M*·ADP states, the simulated EPR transients (Figures 6 and 7, solid line, bottom) overlay the transient EPR data very well (Figures 6 and 7, open boxes, bottom). If the population of the mobile component were due to the population of the M*·ATP state, the simulated EPR transient would resemble the kinetic simulations of the M*·ATP state. For example, at pH 7.0, the EPR intensity would increase to the level of V^{**} within 10 ms, and then decrease to the steady-state ATPase level. Therefore, the original assignments of the immobile component to the M*·ATP state, and the mobile component to M**·ADP·P_i state, during steady-state ATP hydrolysis (Barnett & Thomas, 1987), are correct.

DISCUSSION

Summary and Interpretation of Results. The purpose of this investigation is to use steady-state and transient EPR to detect distinct conformational states of IASL-S1, distinguished by different probe mobilities, and to correlate these conformational states with specific biochemical intermediates on the myosin ATPase pathway. The motional resolution of the nitroxide EPR spectrum makes spin-labels uniquely powerful in the study of the molecular dynamics of systems with more than one motional class. Steady-state EPR spectroscopy has the ability to (a) resolve more than one motionally distinct class of spin-labels and (b) quantitate the relative concentrations of the motional classes. This is critical for the analysis of kinetic mechanisms involving transitions among several conformational states. Transient EPR has the same advantages as steady-state EPR, plus the advantage of time resolution, which allows for (a) the measurement of the rate constants for the population of different states on the reaction pathway and (b) the detection of transient intermediates. Therefore, the combination of steady-state EPR, transient EPR, and transient biochemical kinetics allows for the unambiguous correlation of the observed conformational states with specific biochemical intermediates.

The IASL-S1 ATPase cycle was initiated by the flash photolysis of caged ATP [for a review of caged compounds, see McCray and Trentham (1989)]. Previous studies using caged ATP and transient EPR have investigated spectroscopic changes that occur on the 0.5-s–1-s time scale (Berger et al., 1989; Fajer et al., 1990; Lewis & Thomas, 1991; Ostap & Thomas, 1991; Thomas et al., 1992). Those studies used multiple laser flashes and long instrumental time constants (>0.5 s) that allowed for the detection of spectroscopic signals during the steady-state phase of ATP hydrolysis. In the present study, we have made technical advances that include intense (150 mJ/cm^2), single-pulse (10 ns) laser flashes and millisecond instrumental time constants that allow us to detect changes in the rotational dynamics of IASL-S1 during the pre-steady-state phase of ATP hydrolysis. *These advances have made it possible for the direct observation of the dynamic sequence of structural changes in the myosin head during the binding and hydrolysis of ATP.*

The rate constants for the ATPase reaction (Scheme I) of specifically and completely labeled S1 were determined to allow for the rigorous correlation of the steady-state and transient EPR spectra with specific biochemical states of IASL-S1. In the preparations used in this study, the high-salt ATPases and the double integration of the EPR spectra clearly indicate that virtually every S1 is labeled specifically at only SH_1. Therefore, the kinetic rate constants determined for this preparation are representative of only IASL-S1 labeled at SH_1, not a heterogeneous population of labeled and unlabeled S1.

The rate constants determined for the IASL-S1 ATPase reaction were not significantly different from the rate constants reported for iodoacetamide-labeled S1 (Sleep et al., 1981), indicating that conjugation of the TEMPO (free-radical) group to iodoacetamide does not further perturb the ATPase reaction. Like iodoacetamide, the attachment of IASL to SH_1 results in three major perturbations of the ATPase cycle (Scheme I): (a) a decrease in the rate ($k_{+3} + k_{-3}$) of ATP hydrolysis; (b) a decrease in the equilibrium constant (K_3) of the ATP hydrolysis step; and (c) an increase in the rate of the product release step (k_4). The major result of these perturbations is the shift of the predominant steady-state intermediate from the M**·ADP·P_i state to the M*·ATP state. This shift of the predominant steady-state intermediate to the M*·ATP state, a weak-binding configuration of the myosin head, may be responsible for the decrease in isometric tension of spin-labeled muscle fibers (Matta & Thomas, 1992).

The steady-state transient EPR spectra report mobilization of the spin-label upon the addition of nucleotides to IASL-S1 (Figure 2, Table II). This mobilization is not due to an overall change in the rate of rotation of the myosin head, but it is due to internal conformational changes that either (a) mobilize Cys-707 on the nanosecond time scale or (b) change the protein environment surrounding the spin-label, allowing the probe to undergo large-amplitude nanosecond rotational motion (Table II).

The motional resolution inherent in a conventional EPR spectrum allows us to resolve and quantitate the mole fractions of three distinct conformational states of the myosin head (Figure 2, Table II). Digital analysis of the spectrum of IASL-S1 + ATP indicates that the spectrum corresponds to a linear combination of two motionally distinct conformational states (Figure 3, Table III). Conformational states other than the immobile and mobile states are not populated significantly in the steady-state. These conformational states can be correlated with the predominant intermediates present during steady-state ATP hydrolysis, as demonstrated previously (Barnett & Thomas, 1987).

To correlate unambiguously the conformational states observed during steady-state ATP hydrolysis with specific kinetic intermediates, transient EPR experiments were performed (Figures 6 and 7). Direct comparisons of the transient EPR data with the kinetic data were made by creating simulated EPR transients. The simulated EPR transients were constructed by a linear combination of the mole fractions of the predominant biochemical intermediates (see Results), weighted by the spectral contribution of each motional component (V^* and V^{**}, Figures 6 and 7). The linear combinations of the simulated biochemical intermediates show that the assignments of the immobile component to the M*·ATP state and the mobile component to the M**·ADP·P_i state are correct (Figures 6 and 7, bottom). The M*·ADP state also contributes to the population of the immobile component. However, the M*·ADP state makes up less than 10% of the total population of IASL-S1 in the steady state and does not contribute significantly to the spectral changes in the EPR transients.

The EPR transients report the population of both the mobile and immobile components (V^{tot}, see Results), so if the populations of these components occur at different rates, biphasic transients would be expected. At pH 7.0, the EPR transient is clearly biphasic (Figure 6, bottom, boxes). At pH 8.0, the two phases of the transient are not resolved and can be fit to a single exponential (Figure 7, bottom, boxes). The EPR transient at pH 7.0 is biphasic because it is reporting (A) the fast population of the immobile component (M*·ATP state) and (B) the slower population of the mobile component (M**·ADP·P_i state). However, at pH 8.0, the photolysis rate of caged ATP (k_{caged}) is 10× time slower than at pH 7.0, so the rate of ATP binding to IASL-S1 (10 s^{-1}) and the subsequent population of the M*·ATP state are comparable to the rate of population of the M**·ADP·P_i state (26 s^{-1}). Therefore, the EPR transient at pH 8.0 is monophasic because the rates of ATP binding and hydrolysis are approximately equivalent.

The transient EPR data (a) demonstrate that the conformational states are populated at the same rates as the biochemical states and (b) exclude the possibility of the

presence of other conformational intermediates during the pre-steady-state phase of ATP hydrolysis. These assignments confirm the identifications made previously using steady-state kinetics and nucleotide analogs (Seidel & Gergely, 1971; Barnett & Thomas, 1987).

Relationship to Other Work. Although we can determine the rate and amplitude of spin-label mobility (Table II), and the rate and extent of the population of the motionally distinct states (Table III, Figures 5 and 6), we cannot describe the exact nature of the structural changes being detected. However, we can correlate the spectroscopic changes observed in this study with investigations that have measured structural changes in the myosin head.

Fluorescence anisotropy decay (Aguirre et al., 1989), transient electrical birefringence (Highsmith & Eden, 1990, 1993), and small-angle X-ray scattering (Wakabayashi et al., 1992) have detected significant changes in the overall shape of the myosin head as a function of bound nucleotide. It was determined that the radius of gyration of S1 decreases in the presence of ATP or ATP + V_i, indicating that the myosin head is more compact in the M**·ADP·P_i state. The small-angle X-ray scattering studies indicated that the shape of S1 is significantly different in the absence of nucleotide, in the presence of ADP, and in the presence of ADP + V_i (Wakabayashi et al., 1992). This is consistent with the three distinct conformations of the myosin head that we have resolved in the present study. Hydrodynamic modeling of the myosin head indicates that one end of the myosin molecule may move up to 4 nm upon the binding and hydrolysis of ATP (Wakabayashi et al., 1992; Highsmith & Eden, 1993). This movement has been proposed to be associated with the force-generating power stroke (Wakabayashi et al., 1992; Highsmith & Eden, 1993).

Changes in the shape of the myosin head have also been observed by electron microscopy upon the binding of ATP and ATP analogs (Walker & Trinick, 1988; Katayama, 1989; Tokunaga et al., 1991). These conformational changes have been proposed to occur at the SH_1 region between the 20K and 50K fragments of the myosin head (Tokunaga et al., 1991). Biochemical cross-linking studies demonstrate that the region containing SH_1 and SH_2 can move >10 Å upon ATP binding, indicating that this 11 amino acid section of the myosin heavy chain possesses extraordinary flexibility (Huston et al., 1988). Therefore, it is likely that the IASL covalently bound to SH_1 is detecting conformational changes in the 20K fragment that accompany large-scale changes in the myosin head structure that may be related to the myosin power stroke. The high-resolution crystal structure of the myosin head will allow for a more complete interpretation of these results (Winkelman et al., 1991; Rayment, 1993). We have been able to correlate directly these conformational states with specific biochemical intermediates on the myosin ATPase pathway, and we have established the technology to detect myosin's conformational states in muscle fibers during muscle contraction.

Conclusions. The steady-state EPR experiments resolved three distinct conformational states of the myosin head, and the transient EPR experiments allowed for the direct correlation of the conformations with transient biochemical kinetics of the millisecond time scale. The conformationally distinct states corresponded to the no-nucleotide, M*·ATP, and M**·ADP·P_i biochemical states. These transient EPR studies will be extended to myofibrils and skinned fibers, in which specific labeling of SH_1 has been achieved with IASL (Thomas & Cooke, 1980). Thus, transient EPR offers the first opportunity to detect and resolve myosin's conformational transients in fibers during muscle contraction (Matta & Thomas, 1992; Ostap et al., 1993). Transient EPR will also allow for the transient detection of the global dynamics and orientation of myosin (Cooke et al., 1982; Barnett & Thomas, 1989; Roopnarine et al., 1993) and actin (Naber et al., 1992; Ostap et al., 1992) in muscle fibers.

ACKNOWLEDGMENT

We thank C. L. Berger, J. E. Mahaney, V. A. Barnett, and Y. E. Goldman for helpful discussions, R. L. H. Bennett, F. L. Nisswandt, B. Belknap, and A. Robinson for technical assistance, and J. C. Voss for assistance in the purification of caged ATP. We also thank David Trentham for critically reviewing the manuscript.

REFERENCES

Aguirre, R., Lin, S. H., Gonsoulin, F., Wang, C. K., & Cheung, H. C. (1989) *Biochemistry 28*, 799–807.
Bagshaw, C. R., & Trentham, D. R. (1974) *Biochem. J. 141*, 331–379.
Barnett, V. A., & Thomas, D. D. (1987) *Biochemistry 26*, 314–323.
Barnett, V. A., & Thomas, D. D. (1989) *Biophys. J. 56*, 517–523.
Berger, C. L., & Thomas, D. D. (1991) *Biochemistry 30*, 11036–11045.
Berger, C. L., Svensson, E. C., & Thomas, D. D. (1989) *Proc. Natl. Acad. Sci. U.S.A. 86*, 8753–8757.
Cooke, R., Crowder, M. S., & Thomas, D. D. (1982) *Nature (London) 300*, 776–778.
Crowder, M. S., & Cooke, R. (1984) *J. Muscle Res. Cell Motil. 5*, 131–146.
Dalbey, R. E., Weiel, J., & Yount, R. G. (1983) *Biochemistry 22*, 4696–4706.
Dantzig, J. A., & Goldman, Y. E. (1985) *J. Gen. Physiol. 86*, 305–327.
Eads, T. M., Thomas, D. D., & Austin, R. H. (1984) *J. Mol. Biol. 179*, 55–81.
Eisenberg, E., & Hill, T. L. (1985) *Science 227*, 999–1006.
Fajer, P. G., Fajer, E. A., & Thomas, D. D. (1990) *Proc. Natl. Acad. Sci. U.S.A. 87*, 5538–5542.
Goldman, Y. E., Hibberd, M. G., & Trentham, D. R. (1984) *J. Physiol. 354*, 577–604.
Goodno, C. C. (1979) *Proc. Natl. Sci. U.S.A. 76*, 2620–2624.
Hibberd, M. G., & Trentham, D. R. (1986) *Annu. Rev. Biophys. Biophys. Chem. 15*, 119–161.
Highsmith, S., & Eden, D. (1990) *Biochemistry 29*, 4087–4093.
Highsmith, S., & Eden, D. (1993) *Biochemistry 32*, 2455–2458.
Hiratsuka, T. (1992) *J. Biol. Chem. 21*, 14941–14948.
Huston, E. E., Grammer, J. C., & Yount, R. G. (1988) *Biochemistry 27*, 8945–8952.
Huxley, A. F., & Simmons, R. (1971) *Nature (London) 233*, 533–538.
Huxley, H. E. (1969) *Science 164*, 1356–1366.
Johnson, K. A., & Taylor, E. W. (1978) *Biochemistry 17*, 3432–3442.
Katayama, E. (1989) *J. Biochem. 106*, 751–770.
Lanzetta, P. A., Alvarez, L. J., Reinach, P. S., & Candia, D. A. (1979) *Anal. Biochem. 100*, 95–97.
Lewis, S. M., & Thomas, D. D. (1991) *Biochemistry 30*, 8331–8339.
Margossian, S. S., & Lowey, S. (1982) *Methods Enzymol. 85*, 55–71.
Matta, J. J., & Thomas, D. D. (1992) *Biophys. J. 61*, A295.
McCalley, R. C., Shimshick, E. J., & McConnell, H. M. (1972) *Chem. Phys. Lett. 13*, 115–119.
McCray, J. A., & Trentham, D. R. (1989) *Annu. Rev. Biophys. Biophys. Chem. 18*, 239–270.

McCray, J. A., Herbette, L., Kihara, T., & Trentham, D. R. (1980) *Proc. Natl. Acad. Sci. U.S.A. 77*, 7237–7241.
Morita, F. (1967) *J. Biol. Chem. 242*, 4501–4506.
Naber, N., Ostap, E. M., Thomas, D. D., Wieland, T., Cooke, R. (1992) *Biophys. J. 61*, 303a.
Ostap, E. M., & Thomas, D. D. (1991) *Biophys. J. 59*, 1235–1241.
Ostap, E. M., Yanagida, T., & Thomas, D. D. (1992) *Biophys. J. 63*, 966–975.
Ostap, E. M., Barnett, V. A., & Thomas, D. D. (1993) *Biophys. J. 63*, A361.
Press, W. H., Flannery, B. P., Teukolsky, S. A., & Vetterling, W. T. (1987) in *Numerical Recipes*, pp 550–560, Cambridge University Press, Cambridge, U.K.
Rayment, I. (1993) *Biophys. J. 64*, A2.
Roopnarine, O., Hideg, K., & Thomas, D. D. (1993) *Biophys. J.* (in press).
Reedy, M. K., Holmes, K. C., & Tregear, R. T. (1965) *Nature (London) 297*, 1276–1280.
Seidel, J. C. (1975) *J. Biol. Chem. 250*, 5681–5687.
Seidel, J. C., & Gergely, J. (1971) *Biochem. Biophys. Res. Commun. 44*, 826–830.
Seidel, J. C., & Gergely, J. (1973) *Arch. Biochem. Biophys. 158*, 853–863.
Seidel, J. C., Chopek, M., & Gergeley, J. (1970) *Biochemistry 9*, 3265–3272.
Sekine, T., & Kielly, W. W. (1964) *J. Biochem. (Tokyo) 54*, 196–198.
Shriver, J. W., & Sykes, B. D. (1982) *Biochemistry 21*, 3022–3028.
Sleep, J. A., Trybus, K. M., Johnson, K. A., & Taylor, E. W. (1981) *J. Muscle Res. Cell Motil. 2*, 373–399.
Squier, T. C., & Thomas, D. D. (1986) *Biophys. J. 49*, 921–935.
Squier, T. C., & Thomas, D. D. (1989) *Biophys. J. 56*, 735–748.
Sutoh, K., & Lu, R. C. (1987) *Biochemistry 26*, 4511–4516.
Taylor, E. W. (1979) *CRC Crit. Rev. Biochem. 6*, 103.
Thomas, D. D., & Cooke, R. C. (1980) *Biophys. J. 32*, 891–806.
Thomas, D. D., Seidel, J. C., Hyde, J. S., & Gergely, J. (1975) *Proc. Natl. Acad. Sci. U.S.A. 72*, 1729–1733.
Thomas, D. D., Ostap, E. M., Berger, C. L., Lewis, S. M., Fajer, P. G., & Mahaney, J. E. (1993) *Biol. Magn. Reson. 13*, 323–351.
Tokunaga, M., Sutoh, K., & Wakabayashi, T. (1991) *Adv. Biophys. 27*, 157–167.
Trentham, D. R., Eccleston, J. F., & Bagshaw, C. R. (1976) *Q. Rev. Biophys. 9*, 217–281.
Wakabayashi, K., Tokunaga, M., Kohno, I., Sugimoto, Y., Hamanaka, T., Takezawa, Y., Wakabayashi, T., & Amemiya, Y. (1992) *Science 258*, 443–447.
Walker, J. W., Reid, G. P., McCray, J. A., & Trentham, D. R. (1988) *J. Am. Chem. Soc. 110*, 7170–7177.
Walker, M., & Trinick, J. (1988) *J. Muscle Res. Cell. Motil. 9*, 359–366.
Wells, C., & Bagshaw, C. R. (1984) *J. Muscle Res. Cell Motil. 5*, 97–112.
Werber, M., Szent-Györgyi, A. G., & Fasman, G. (1972) *Biochemistry 11*, 2872–2882.
White, H. D. (1982) *Methods Enzymol. 85*, 698–708.
Winkleman, D. A., Baker, S. B., & Rayment, I. (1991) *J. Cell Biol. 114*, 701–713.